

Research on the Influence of Wheel Tread Defects on Rolling Contact Fatigue

Ze Li¹, Xue-cheng Ping^{2,*}

^{1,2} College of Mechanical Engineering, Tianjin University of Science and Technology, Tianjin 300222, China

^{1,2} Tianjin Key Laboratory of Integrated Design and Online Monitoring of Light Industry and Food Engineering Machinery Equipment, Tianjin University of Science and Technology, Tianjin 300222, China

¹ 2578924527@qq.com, ² xcping@tust.edu.cn

*Correspondence Author

Abstract: *With the rapid development of high-speed trains, local rolling contact fatigue caused by special local defect damage forms has become more prominent. This article takes circular defects as the research object, adopts the Jiang Sehitoglu multi-axis fatigue damage criterion based on the critical plane method, establishes a finite element model of wheel tread circular defects, and studies the influence of wheel tread circular defects on wheel rail rolling contact fatigue. Based on finite element analysis to obtain fatigue damage parameters, an improved PSO-BP neural network was used to establish a neural network prediction model for fatigue damage parameters, and the feasibility of the model was demonstrated. The research results show that the main influencing factors on the rolling contact fatigue life of wheel tread defects are shear stress and shear strain; The fatigue damage parameter is maximum at the edge of the wheel tread defect; As the defect distribution moves from the center to both sides, the contact stress and damage parameters gradually decrease; As the depth of the defect increases to the size of the radius, the contact stress and damage parameters first increase and then decrease; As the diameter of the defect increases, the contact stress and damage parameters increase, but the amplitude change gradually tends to stabilize with the increase of the defect diameter. The neural network prediction results indicate that all predicted samples are within a reasonable range, and this neural network model can provide a reference for predicting fatigue damage of wheel tread.*

Keywords: Wheel tread defects, Rolling contact fatigue, Defective geometric structure, BP neural network.

1. Introduction

With the rapid development of the economy, railway transportation has become one of the indispensable modes of transportation in China. The wheel-rail system, as a key component in railways, is subjected to a very complex mechanical environment in its contact area. The rolling of the wheels causes the contact area to be subjected to repeated cyclic forces, ultimately leading to material fatigue damage and failure [1-3]. As a key component of maintaining smooth train operation, the appearance of surface defects on the wheel-rail can accelerate the formation and expansion of nearby cracks, which may lead to damage, instability, and even accidents in the train wheel-rail system, seriously threatening the safety of high-speed trains.

With the development of production technology and the improvement of material fatigue performance, the RCF caused by material performance defects and wear of the wheel-rail itself has been effectively suppressed, while the local rolling contact fatigue caused by special local defect damage forms appears more prominent and random [4-6]. The generation of defects will have a significant impact on the performance of wheel-rail usage, including the impact strengthening of the microstructure of the materials around the defects, changes in the wheel-rail contact state, and changes in the distribution of contact stress. Therefore, it is necessary to establish and improve the theoretical and technical support for the fatigue damage problem of wheel-rail surface defects based on the size and morphology of the defects [7]. Zeng et al. [8] used FS damage parameters combined with the critical plane method to study the initiation of fatigue cracks and found that pre-rolling is more likely to cause the initiation of surface defect RCF cracks in wheel steel. They determined the critical defect size for the initiation of RCF cracks in pre-rolled wheel discs. An et al. [9]

established a three-dimensional finite element model to simulate the transient rolling behavior of wheelsets on a straight track, explored the influencing factors of plastic deformation of wheel tracks, and obtained the conditions for different scratch morphologies. Zhao and others [10-11] used a self-made pendulum impact mechanism to prepare surface damage pits of different shapes and sizes. By comparing macroscopic experimental data such as sample wear and hardness, as well as microscopic perspectives such as surface damage morphology and profile fatigue damage, the influence of the size of circular damage pits on the propagation behavior of rolling contact fatigue cracks in steel rails was analyzed. Establish wear damage mechanism diagrams and fatigue damage mechanism diagrams for two types of defects, and propose the critical defect size that causes severe fatigue cracks on the surface of the rail. Jungwon et al. [12] used double disc tests and finite element analysis to introduce artificial defects to study the rolling contact fatigue damage on the surface of steel rails. They found that when the defect diameter is shorter than a certain length, it will disappear due to wear, and large-sized dents and cracks, will initiate and propagate, ultimately leading to the detachment of large blocks.

As a powerful machine learning model, neural networks can handle complex nonlinear relationships and have unique advantages in fatigue life prediction. In recent years, they have been applied by more scholars in the field of fatigue. Xu et al. [13] proposed a fatigue life prediction method based on the RBF neural network, which improved the model accuracy by optimizing the target and diffusion values of the neural network. Wang [14] constructed different neural network algorithms and found that it is feasible to convert the theoretical stress concentration coefficients of different standard components under various load conditions into sequential data as the size ratio changes. Zhang [15]

constructed a multi-axis fatigue life prediction model for metal materials based on fully connected neural networks. Compared with traditional prediction models, it can achieve higher prediction accuracy. Dou et al. [16] proposed three algorithms to optimize the BP neural network model and found that the quasi-Newton algorithm had the highest prediction accuracy. Based on this, they proposed a continuous pipe life interval prediction, and the prediction structure met the accuracy requirements.

In recent years, domestic and foreign scholars have conducted in-depth research on different types of surface defects through experimental methods, but there is little analysis of wheel-rail rolling fatigue through neural networks. This article is based on the multi-axis fatigue criterion of the critical plane method and establishes a finite element model of wheel-rail rolling fatigue with wheel tread defects. Using sub-model technology, the influence of changes in defect distribution position, depth, and diameter on contact state and damage parameters is discussed. A fatigue damage prediction model is established based on the BP neural network, and the model accuracy can meet the requirements of fatigue damage prediction.

2. Multiaxial Fatigue Criterion

In rolling contact fatigue problems, the contact surface is not only affected by contact pressure and cyclic load but also by frictional shear force. This complex stress state makes it difficult to predict the location and direction of crack initiation, and the critical plane method is one of the methods for studying multi-axis fatigue crack initiation. It is believed that cracks will initiate on a specific dangerous plane, which is called the maximum damage plane, and the parameters used to evaluate this plane are called fatigue damage parameters. By calculating fatigue damage parameters, the key factors affecting the fatigue life of materials under multiaxial loads can be determined [17]. In rolling contact fatigue, the tensor directions of stress and strain will change over time. The critical plane method can quickly search for this dangerous plane at a critical location, and rolling fatigue failure often occurs on this plane [18-20].

Obtain the stress and strain values of all nodes under all incremental steps through finite element analysis. In three-dimensional coordinates, the stress and strain components at any point can be written in the following form:

$$\sigma = \begin{bmatrix} \sigma_{xx} & \tau_{xy} & \tau_{xz} \\ \tau_{xy} & \sigma_{yy} & \tau_{yz} \\ \tau_{xz} & \tau_{yz} & \sigma_{zz} \end{bmatrix} \quad (1)$$

$$\varepsilon = \begin{bmatrix} \varepsilon_{xx} & \gamma_{xy} & \gamma_{xz} \\ \tau_{xy} & \varepsilon_{yy} & \gamma_{yz} \\ \gamma_{xz} & \gamma_{yz} & \varepsilon_{zz} \end{bmatrix} \quad (2)$$

Where σ and ε are matrices of stress and strain components. σ_{xx} , σ_{yy} , and σ_{zz} are normal stress components. τ_{xy} , τ_{xz} , and τ_{yz} are the shear stress components. ε_{xx} , ε_{yy} , and ε_{zz} are positive strain components. γ_{xy} , γ_{xz} , and γ_{yz} are the shear strain components.

By rotating coordinates, the stress and strain components on any cross-section can be obtained. The new coordinate system after rotation is obtained by rotating the original coordinate

system counterclockwise around the X-axis, Y-axis, and Z-axis by angles of α , φ , and θ . In a three-dimensional stress state, the phase of any material plane can be determined by the normal vector of that material plane. The stress tensor on the material plane can be calculated using the following formula:

$$\sigma' = (M)^T \sigma (M) \quad (3)$$

$$\varepsilon' = (M)^T \varepsilon (M) \quad (4)$$

Where M^T is the transpose of the transformation matrix M . The expression for M is as follows:

$$M = \begin{bmatrix} \cos \varphi & 0 & \sin \varphi \\ \sin \alpha \sin \varphi & \cos \alpha & -\sin \alpha \cos \varphi \\ -\cos \alpha \sin \varphi & \sin \alpha & \cos \alpha \cos \varphi \end{bmatrix} \quad (5)$$

In engineering practice, to more accurately predict the fatigue life of materials, many fatigue life prediction models based on the critical plane method have been proposed. According to the different parameters defining the maximum damage plane, they can be divided into the following types:

Jiang and Sehitoglu [21-22] improved the critical plane definition method proposed by Findley, stating that the critical interface is not only affected by normal stress but also by shear stress and average normal stress. Based on this, an improved FP damage parameter model was proposed:

$$FP = \langle \sigma_{n,max} \rangle \frac{\Delta \varepsilon_n}{2} + J \Delta \tau \Delta \gamma \quad (6)$$

In the formula: $\langle \rangle$ represents MacCauley parentheses, $\langle x \rangle = 0.5 (|x| + x)$; $\sigma_{n,max}$ is the maximum normal stress, $\Delta \varepsilon_n$ is the full amplitude of normal strain; $\Delta \tau$ and $\Delta \gamma$ are the full amplitude of maximum shear stress; J is the material constant measured experimentally.

Fatemi and Society [23] proposed a correction parameter based on linear cumulative damage theory, which takes into account amplitude and average stress. The components of this correction parameter are composed of the maximum shear strain amplitude and the maximum normal stress on the maximum shear strain amplitude plane. The expression for the FS parameter is:

$$FS = \frac{\Delta \gamma}{2} \left(1 + \frac{\sigma_{n,max}}{\sigma_y} \right) \quad (7)$$

σ_y is the yield strength of the material, k is the material constant.

Smith and Watson [24] proposed a stress-strain function, which demonstrated a simple relationship between the fatigue life of the specimen and the proposed stress-strain parameter by testing the correlation between the stress-strain function and the fatigue life of different materials. This parameter can be defined as the product of the maximum normal stress $\sigma_{n,max}$ and the maximum normal strain amplitude $\Delta \varepsilon_{max}/2$, and its expression is:

$$SWT = \sigma_{n,max} \frac{\Delta \varepsilon_{max}}{2} \quad (8)$$

3. Finite Element Model

3.1 Model

The dimensions of the wheel model follow the relevant design

criteria of TB/T 1010-2016. The tread diameter is 950 mm, and the center hole diameter is 170 mm. The dimensions of the rail model are determined according to the relevant design criteria of TB/T 3276-2011.

Using ABAQUS finite element software for modeling. The wheels are made of ER8 steel, and the rails are made of U71MnG steel, both of which are isotropic materials. The properties of wheel-rail materials are shown in Table 1. The contact surface adopts universal contact, and the penalty function is used to define the friction coefficient in the tangential direction. The friction coefficient is 0.3[25], and hard contact is used in the normal direction. An RP reference point is established at the center of the wheel, which is

coupled with the center of the wheel through coupling constraints. All external loads and boundary conditions are applied to this reference point. To improve computational efficiency, precise stress analysis is only performed using fine grids in the contact area, with a minimum grid size of 2 mm x 2 mm x 2 mm. The rail model is fixed at both ends and bottom. Figure 1 shows a three-dimensional wheel rail model and its mesh division established using UG software. The entire model adopts a hexahedral mesh, and the mesh element type is the C3D8R element.

Table 1: Main Material Properties of Wheel Rail

Component	Material	Elastic modulus/GPa	Poisson's ratio	Density/kg/m ³
Wheel	ER8	210	0.3	7.80×10 ³
Rail	U71MnG	208	0.27	7.85×10 ³

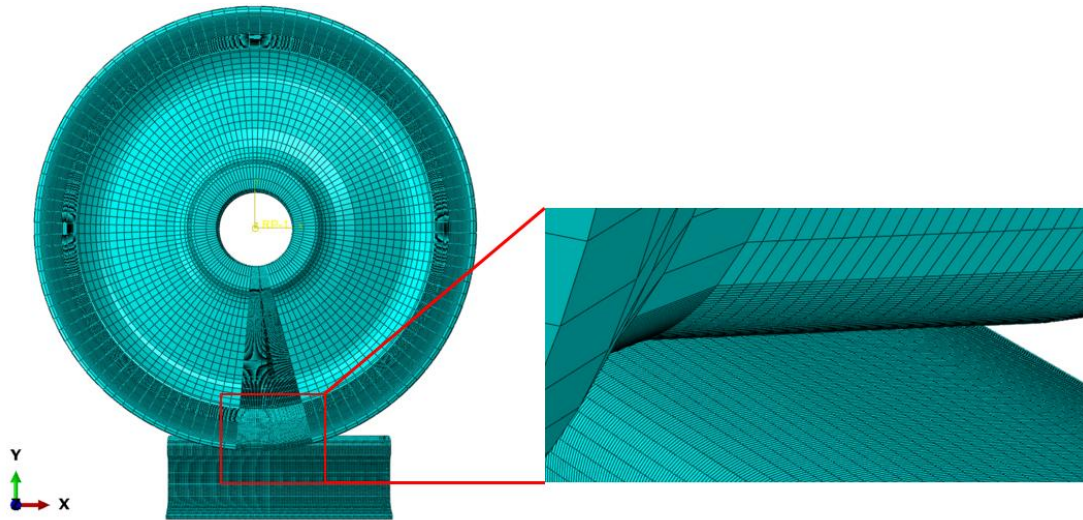


Figure 1: Mesh division of finite element model for wheel rail rolling contact

The model analysis is divided into two steps. The first step is the axle-to-wheel compression condition, and the second step is the wheel linear rolling condition. To ensure the convergence of the calculation results, geometric nonlinearity is enabled and the initial incremental step time is set as small as possible to reduce the difficulty of convergence.

above and obtain the finite element analysis results for each step. Considering that the wheel is a centrally symmetrical component and the contact area is relatively small compared to other areas, a 20° range is divided above the wheel to form a sub model as shown in Figure 2. In this sub-model, typical dimensions of the wheel tread defects were selected and the defects were designed on the submodel.

Perform finite element analysis on the entire model mentioned

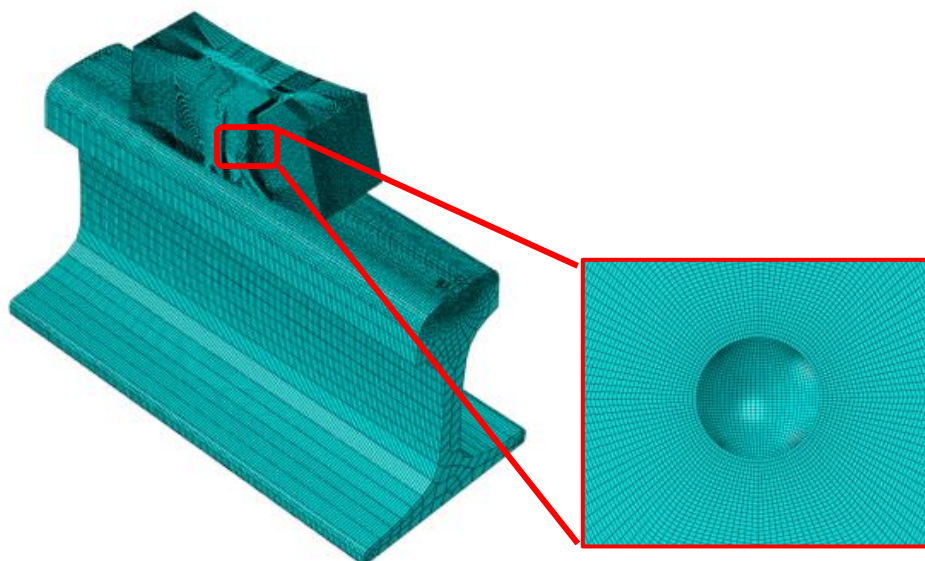


Figure 2: Mesh division of finite element submodel for wheel rail defects

This article takes circular defects as the research object. Without considering residual stress, circular defects with different distribution positions, depths, and diameters are introduced on the road tread to analyze the contact stress and

FP fatigue damage parameters under the influence of different geometric parameters.

3.2 Model Validation

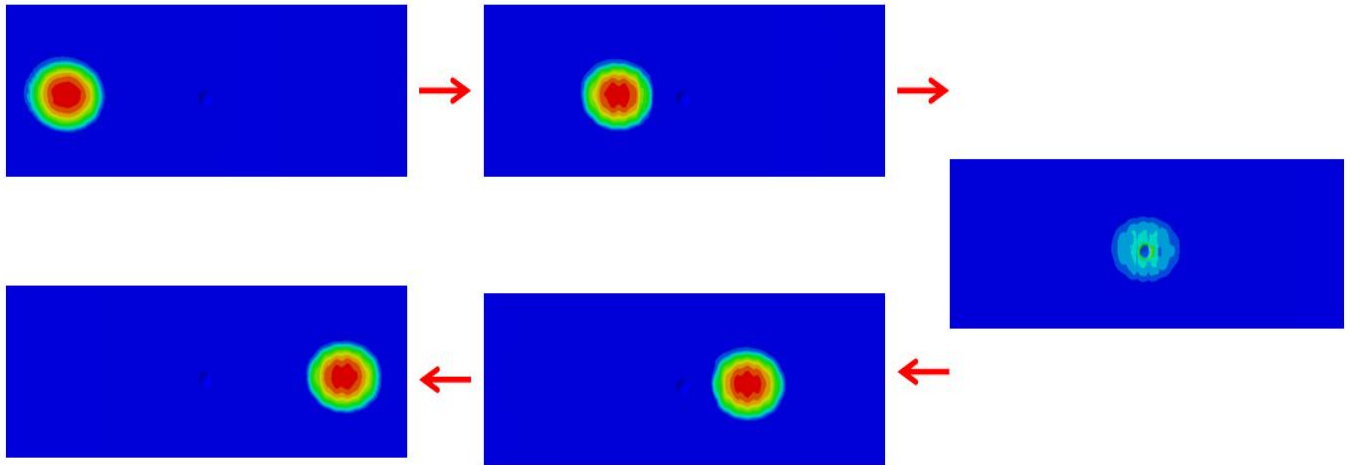


Figure 3: Changes in the position of wheel tread contact spots

Write user subroutines in Fortran language to calculate FP damage parameters. Considering a defect depth of 0.5mm, a defect diameter of 3mm, and a defect distribution position located at the center of the tread, analyze the changes in the FP damage criterion parameters during the rolling process, and determine the critical plane to obtain the crack initiation position and angle. Figure 3 shows the variation of contact stress on the wheel tread during the rolling process. When the wheel rolls without passing through the defect area, the

contact stress is consistent with the analysis results of the defect-free finite element model. However, when the wheel tread passes through the defect area, there is a significant concentration of contact stress. Especially when the wheel rolls just past the middle position of the defect area, the contact stress is most concentrated, reaching a maximum value of 4958MPa. As the wheel gradually moves away from the defect area, the contact stress gradually returns to its original state and ultimately remains stable, with little change.

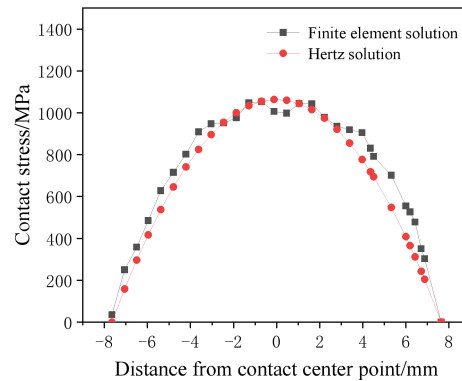
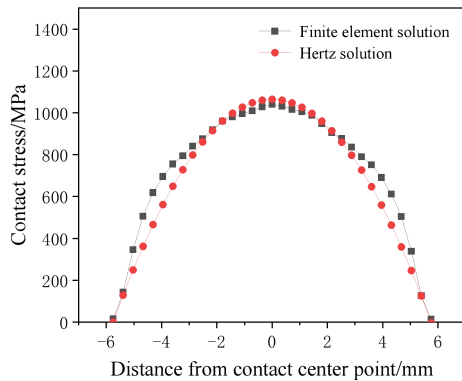


Figure 4: Distribution of wheel rail contact stress: (a) Short axis direction; (b) Long axis direction

The literature [19] points out that when two elastic bodies come into contact, the contact area should have an elliptical contact stress distribution and meet the Hertz contact theory. Figure 4 shows the contact stress distribution obtained from finite element analysis and the contact stress distribution calculated based on Hertz contact theory. As shown in the figure, the contact spot obtained from finite element analysis has a long axis radius of about 7.8 mm and a short axis radius of about 5.8 mm. The distribution pattern is that the pressure gradually decreases from the middle to the surrounding areas. Compared with the distribution solutions calculated by Hertz contact theory, it can be found that although the two distribution shapes are similar, the results obtained by finite element calculation may be slightly larger at certain positions. This is because Hertz contact theory is a distribution law under ideal stress conditions, and the complex structure of the wheel-rail and the imbalance of stress can lead to differences.

3.3 Result Analysis

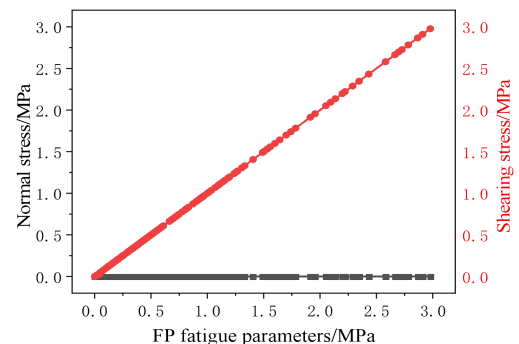


Figure 5: Damage parameters of target surface nodes at different angles

Extracting data from finite element analysis results, combined with the critical plane method and FP damage criterion, can

determine the plane corresponding to the maximum value of FP damage parameters, which is the plane where fatigue cracks originate. After extracting the force and strain data of each unit in the calculation area over time, the fatigue parameters of each unit at different rotation angles can be calculated. Based on Figure 5, it can be seen that when the FP damage parameter is less than 0.05, a small portion of the FP damage parameters at element nodes are jointly affected by tensile and shear stresses. When the FP damage parameter is greater than 0.05, the unit is mainly subjected to shear stress, and the influence of tensile stress on the FP damage parameter can be almost ignored. This phenomenon occurs because during the calculation process, the maximum normal stress is negative, and the result of the normal stress-strain part calculated using MacCauley parentheses is 0. This indicates that shear stress and shear strain $J\Delta\tau\Delta\gamma$ are the main factors affecting fatigue crack initiation.

4. Factors Affecting Rolling Contact Fatigue of Wheel Tread Defects

4.1 Defect Distribution Location

Based on the center position of the circular defect, set the Y-axis as the axial direction of the wheel, and the center position of the wheel tread as the coordinate origin. The given defect distribution range is $-7\text{mm} \leq y_0 \leq 7\text{mm}$, with positive values on the outer side of the wheel and negative values on the inner side. Take a distance increment $\Delta y=1\text{mm}$ in the axial direction to study the effect of defect distribution position on rolling contact fatigue. Apply other identical boundary conditions to the model and ensure that the defect diameter D is 3mm and the depth d is 0.5mm.

Figure 6 shows the variation of contact stress with the analysis step time. As shown in the figure, when the defect area of the wheel tread is not in contact with the steel rail, the contact stress is maintained within a stable range; When rolling through the defect area, the contact stress rapidly increases. Figure 7 shows that as the defect position moves towards both sides of the centerline, the maximum contact stress gradually decreases, and when moving the same distance, the contact stress on the inner side is slightly greater than that on the outer side, which is due to the wheel structure. The closer the defect distribution is to the center of the tread, The larger the FP damage parameter, and the shorter the fatigue life.

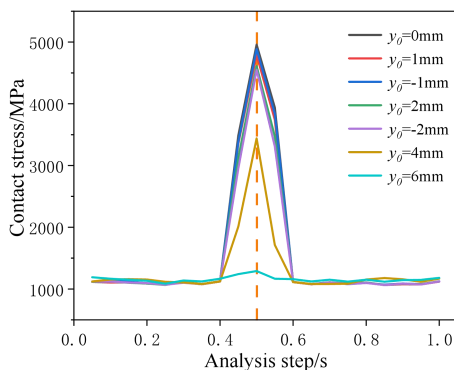


Figure 6: Changes in Contact Stress with Analysis Steps

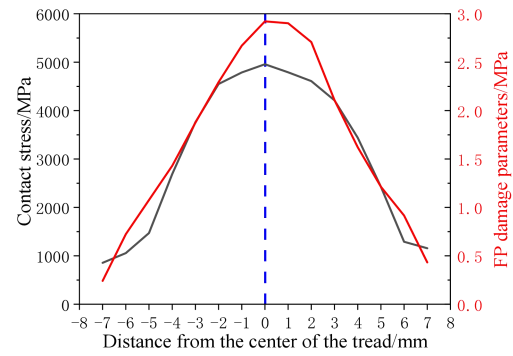


Figure 7: Changes of Different Parameters with Distribution Positions

4.2 Defect Depth

The measure of defect depth is defined as the distance from the surface of the wheel tread to the deepest point of the defect along the radial direction of the wheel, which is d . When the same boundary conditions are applied to the model, the maximum depth that can be produced by different defect diameters will also vary. Assuming the defect diameter D is 3mm, the distance from the center position of the tread y_0 is 0mm, and the range of defect depth d is $0\text{mm} \leq d \leq 1.5\text{mm}$, with an increment of $\Delta d=0.1\text{mm}$.

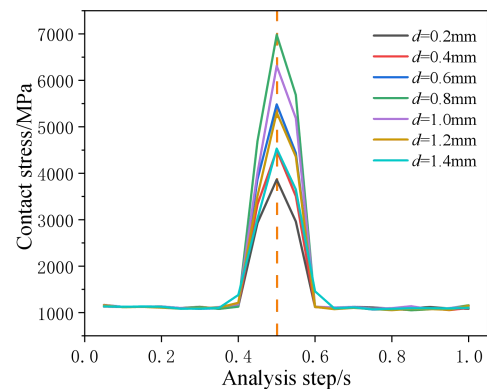


Figure 8: Changes in Contact Stress with Analysis Steps

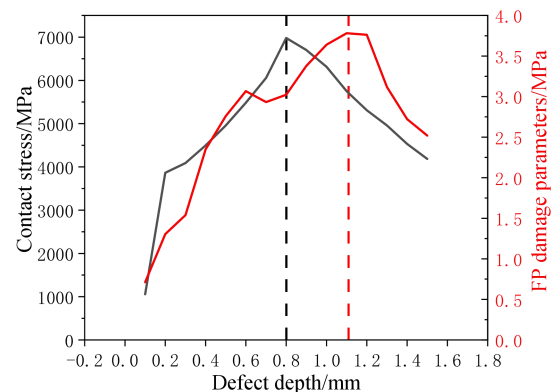


Figure 9: Changes in different parameters with defect depth

Figure 8 and Figure 9 show the parameter changes at different defect depths d under the condition of defect diameter $D=3\text{mm}$ and distribution position $y_0=0\text{mm}$. Figure 8 shows the variation of contact stress with the analysis step. As the depth d increases, the contact stress remains unchanged when the wheel tread defect does not come into contact with the rail; When in contact with the steel rail, the contact stress reaches its maximum value. Figure 9 shows the trend of the maximum

contact stress and FP damage parameter gradually increasing with the increase of depth d when the defect diameter D is 3 mm. As the depth approaches the defect radius, the maximum value gradually decreases.

4.3 Defect Diameter

The defect diameter is defined as the distance between a circular defect and the center of the defect sphere. Apply the same boundary conditions in the model, set the defect distribution position $y_0=0\text{mm}$, and the defect depth $d=0.5\text{mm}$. The defect diameter range is set to $1.5\text{mm} \leq D \leq 4.0\text{mm}$, with a diameter increment of $\Delta D=0.25\text{mm}$.

Figure 10 and Figure 11 show the parameter changes for different defect diameters D under the condition of defect depth d of 0.5mm and defect distribution position y_0 of 0mm. As shown in Figure 11, keeping other conditions constant, as the defect diameter increases, the contact stress remains unchanged when the wheel tread defect does not come into contact with the rail; When in contact with the steel rail, the contact stress reaches its maximum value. From Figure 12, it can be seen that as the defect diameter increases, the contact stress and FP damage parameters gradually increase. As the ratio of defect diameter to depth gradually increases, the amplitude of change in FP damage parameters is almost zero. This is because as the defect diameter increases, the impact on the model structure becomes smaller, leading to a gradual decrease in the variation of FP damage parameters. It can be inferred that the defect diameter has a certain impact on fatigue damage, but as the diameter increases, its effect gradually weakens.

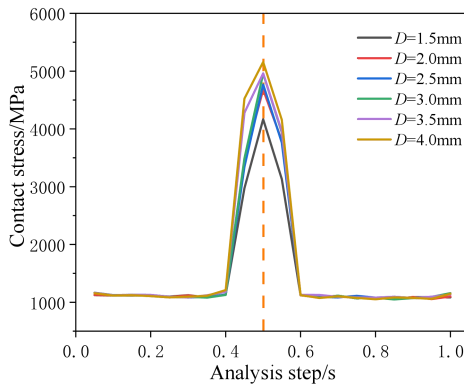


Figure 10: Changes in contact stress with analysis steps

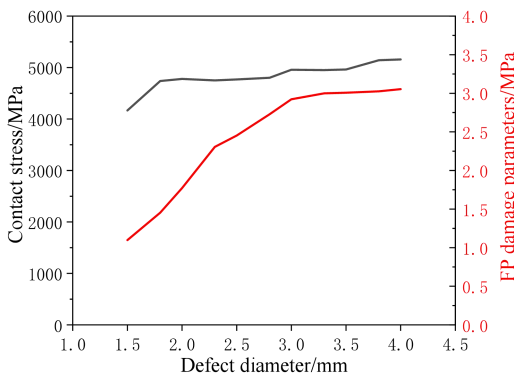


Figure 11: Changes in different parameters with defect diameter

5. Rolling Contact Fatigue Prediction based on Neural Networks

Neural networks can simulate the connectivity and information transmission process between neurons in the human brain, and establish models by learning a large number of data samples, thereby revealing the complex linear relationship between input variables and output variables. This article uses Matlab software to write a program and explores the relationship between defect distribution position, depth, and diameter with rolling contact damage based on an improved PSO-BP neural network.

5.1 Construction of BP Neural Network Model

BP neural network is a multi-layer forward neural network that calculates the error between output and reality, propagates this error back along the network, adjusts weights layer by layer to reduce the error, and repeats until the network converges to a certain error threshold or reaches the maximum number of iterations [26]. Neural networks are divided into input layer, hidden layer, and output layer. Based on the finite element model, determine the defect distribution location, depth, and diameter as input layers, the FP damage parameter is the output layer. The number of hidden layer nodes is determined based on empirical formulas [27]:

$$N_f = \sqrt{m + n} + a \quad (9)$$

In the formula, N_f is the number of hidden layer nodes; n and m are the number of nodes in the input and output layers; a is an integer with a value range of $[0,10]$.

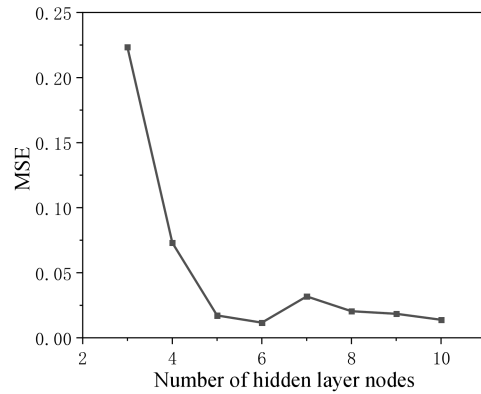


Figure 12: Trend of MSE with the number of hidden layer nodes

Figure 12 shows the trend of mean square error with the number of hidden layer nodes. As shown in the figure, when the number of hidden layer nodes is 6, the BP neural network prediction model has high accuracy. The structure of the neural network model is 3-6-1.

Table 2: Results of tread defect parameters and FP damage parameters

Sample number	y_0/mm	d/mm	D/mm	FP parameters/MPa
1	0	0.5	1.5	1.098
2	0	0.5	1.8	1.453
3	0	0.5	2	1.771
4	0	0.5	2.3	2.306
5	0	0.5	2.5	2.453
6	0	0.3	1.5	1.236
7	0	0.3	1.8	1.529
8	0	0.3	2	1.534
9	0	0.3	2.3	1.59

10	0	0.3	2.5	1.592
11	-2	0.5	1.5	0.862
12	-2	0.5	1.8	1.14
13	-2	0.5	2	1.39
14	-2	0.5	2.3	1.811
15	-2	0.5	2.5	1.926
16	2	0.5	1.5	1.018
17	2	0.5	1.8	1.347
18	2	0.5	2	1.641
19	2	0.5	2.3	2.137
20	2	0.5	2.5	2.273

To ensure prediction accuracy and neural network convergence speed, it is necessary to normalize the data obtained from finite element analysis. Use the randperm function to create a random array to partition the training and testing sets, with a ratio of 4:1 between the training and testing sets. Set the maximum training frequency to 1000 times, with a target error of 10^{-6} and a learning rate of 0.01. Partial finite element analysis data is shown in the table below.

Create a neural network using the newff function, with the hidden layer activation function using the tansig function, which is expressed as:

$$\tan sig(x) = \frac{2}{1+e^{-2x}} - 1 \quad (10)$$

Use the Levenberg-Marquardt algorithm to train neural network models. To further verify the accuracy and reliability of the model calculation, mean square error and correlation coefficient (R^2) were used to evaluate the prediction performance. The smaller the MSE, the closer the correlation coefficient is to 1, and the better the training performance of the neural network:

$$MSE = \frac{1}{n} \sum_{i=1}^n (Y_i - Y_P)^2 \quad (11)$$

$$R^2 = 1 - \frac{\sum_{i=1}^n (Y_i - Y_P)^2}{\sum_{i=1}^n (Y_i - \bar{Y})^2} \quad (12)$$

Y_i is the true value of the i -th sample, Y_P is the predicted value of the model for the i -th sample, n is the number of samples.

5.2 Rolling Fatigue Prediction of Wheel Tread Defects

Based on the finite element analysis results, the total number of samples is 103, with the first 82 groups of analysis results used as the training set for the neural network and the last 21 groups used as the testing set. Based on the determined neural network parameters, considering the defect distribution location, depth, and diameter as the main influencing factors, a BP neural network model is constructed. Figure 13 shows the curve of model iteration times. It is found that when the model iteration times reach 25, the iteration error is the lowest, indicating that the model training has reached the allowed optimal state.

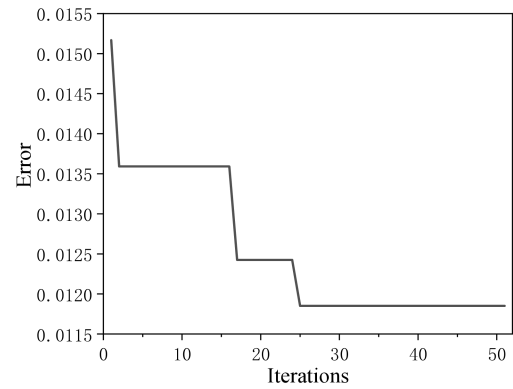


Figure 13: Iteration error varies with the number of iterations

To verify the predictive performance of the trained neural network model on FP damage parameters, two indicators were used to evaluate the predictive performance. Figure 14 and Figure 15 show the comparison curves between the predicted values and finite element values in the training and testing sets. By comparing the training results of the neural network, it can be seen that the numerical values of the predicted values and finite element values are similar, with only a few values showing significant differences. The value of the training set evaluation parameter MSE is approximately 0.0092 and the value of R^2 is approximately 0.9898. The value of the evaluation parameter MSE in the test set is approximately 0.0082 and the value of R^2 is approximately 0.987. This indicates that the established BP neural network model can effectively predict fatigue damage parameters with different defect structures, and the predicted results can maintain good consistency with the finite element results.

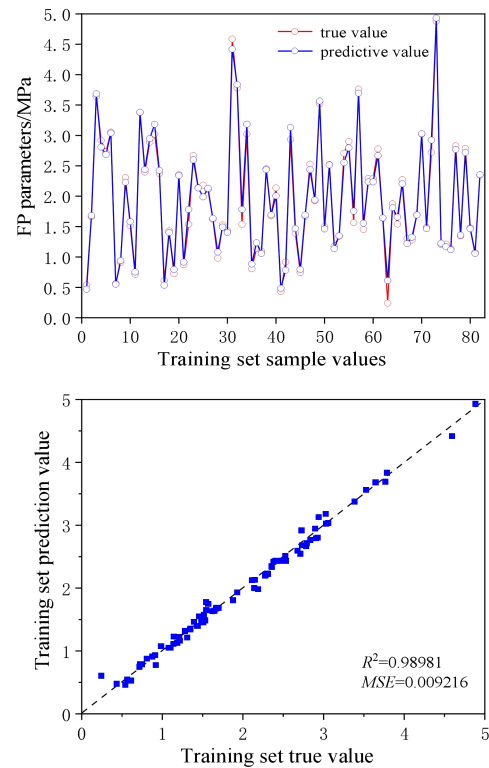


Figure 14: Comparison between predicted and true values in the training set

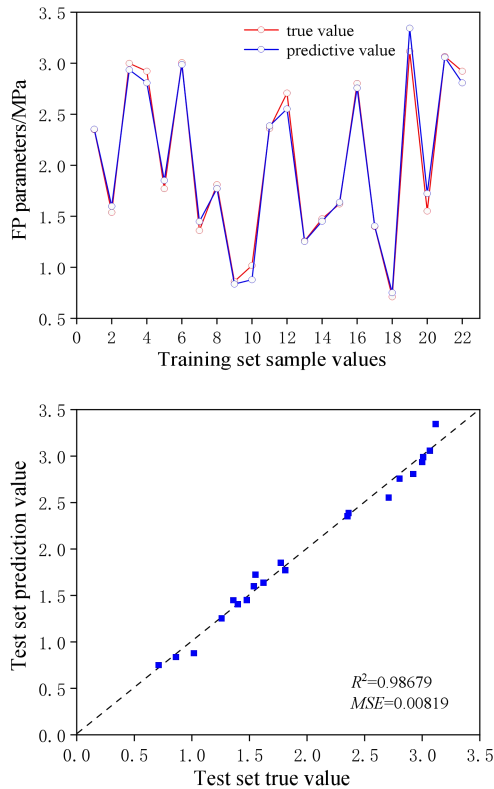


Figure 15: Comparison between predicted and true values in the test set

6. Conclusion

This article explores the effects of different distribution positions y_0 , defect depth d , and defect diameter D on rolling contact fatigue by establishing a finite element model of wheel-rail rolling contact. Analyzed the trend of changes in contact stress and FP damage parameters, proposed a design method for predicting fatigue damage based on the PSO-BP neural network, and established a prediction model through this neural network. The main results are as follows:

(1) The occurrence of defects can lead to stress concentration in the contact stress between the wheel and rail, mainly concentrated at the edge of the defect. The predicted crack initiation location of the wheel tread based on the FP damage criterion is mainly concentrated on the outer edge of the defect. Combining the critical plane method and FP damage criterion, it is found that the main influencing factors on the rolling contact fatigue life of wheel tread defects are shear stress and shear strain.

(2) When the defect is located at the center of the tread, the peak stress and damage parameters reach their maximum values. As the defect moves towards both sides of the wheel, the stress peak and damage parameters will gradually decrease, and the inner peak will be slightly higher than the outer peak, but the peak position will appear on the side near the center; As the depth of the defect gradually increases to the size of the radius, the peak stress and damage parameters will first increase and then decrease, but the peak position will remain unchanged; Increasing the defect diameter will lead to an increase in stress peaks and damage parameters, but as the defect diameter increases, its amplitude gradually approaches zero.

(3) Using the BP neural network to establish a fatigue damage prediction model, the minimum mean square error for prediction is 0.0082, and the maximum correlation coefficient is 0.9898. The BP neural network can achieve the prediction of fatigue damage and meet the accuracy requirements.

References

- [1] Xie Y, Xiao J. Research on the Current Situation and Trends of High Speed Railway Development [J]. High Speed Railway Technology, 2021, 12(02): 23-26.
- [2] Lu C. Research on the initiation mechanism of rolling contact fatigue on the tread of high-speed train wheels [D]. Southwest Jiaotong University, 2015.
- [3] Jin X S, Shen Z Y. Latest progress in research on wheel rail rolling contact fatigue [J]. Journal of Railways, 2001, 23(02): 92-108.
- [4] Zhao X, Wen Z F, Wang H Y, Tao G Q, Jin X S. Research progress on wheel rail rolling contact fatigue in China's rail transit [J]. Journal of Transportation Engineering, 2021, 21(01): 1-35.
- [5] Liu J L, Kan Q H, Wang Y, Zhao J Z, Xu X. Finite element analysis of damage mechanism caused by high-speed train rail abrasion [J]. Journal of Sichuan University of Light Industry and Chemical Technology, 2021, 34(02): 60-69.
- [6] Yin L J. Experimental study on the initiation mechanism of local rolling contact fatigue of wheel rail under impact conditions [D]. Southwest Jiaotong University, 2022.
- [7] Bogdański S. Quasi-static and dynamic liquid solid interaction in 3D squat-type cracks[J]. Wear, 2014, 314(1-2): 20-27.
- [8] Zeng D F, Xu T, Liu W D, Lu L T, Zhang J W, Gong Y H. Investigation on rolling contact fatigue of railway wheel steel with surface defect[J]. Wear, 2020, 446-447: 203207.
- [9] An B Y, Zhao X, Liu C, Wen Z F, Jin X S. Transient rolling contact stress analysis of wheel tread scratches [J]. Lubrication and Sealing, 2014, 39(12): 69-74+79.
- [10] Zhao X J, Ma L, Guo J, et al. The effect of circular abrasion on the rolling contact fatigue characteristics of rail materials under dry water conditions [J]. Journal of Tribology, 2017, 37(04): 544-550.
- [11] Zhao X J. Research on the Influence of Surface Defects on the Rolling Wear and Contact Fatigue Performance of Steel Rails [D]. Southwest Jiaotong University, 2019.
- [12] Jungwon S, Seokjin K, Deonghyeong L. Effects of surface defects on rolling contact fatigue of rail[J]. Procedia Engineering, 2011, 10: 1274-1278.
- [13] Xu Z P, Liu C, Feng H C. Fatigue Life Prediction of Hydraulic Support Front Link Based on Finite Element and RBF Neural Network [J]. Mechanical Design, 2024, 41(01): 110-116.
- [14] Wang S Q. Research on Low Cycle Fatigue Life Prediction Method Based on Neural Networks [D]. Dalian University of Technology, 2022.
- [15] Zhang J. Research on Multi axis Fatigue Life Prediction Model Based on Fully Connected Neural Networks [D]. Guangxi University, 2022.
- [16] Dou Y H, Zhang J Q, Li G L, et al. Prediction of fatigue life of continuous pipes based on optimized BP neural network [J]. Petroleum Machinery, 2023, 51(10): 144-149.

- [17] Karolczuk A, Macha E. A Review of Critical Plane Orientations in Multiaxial Fatigue Failure Criteria of Metallic Materials[J]. *International Journal of Fracture*, 2005, 134(3-4): 267-304.
- [18] Dong Z G. Analysis of the initiation of rolling contact fatigue cracks in high-speed manganese steel fixed frog No. 9 of subway [D]. Southwest Jiaotong University, 2021.
- [19] Li S. Finite element simulation of fatigue crack initiation and propagation characteristics in wheel rail rolling contact [D]. Southwest Jiaotong University, 2021.
- [20] Jonas W R. Life prediction of rolling contact fatigue crack initiation[J]. *International Journal of Fatigue*, 2001, 23(7): 575-586.
- [21] Jiang Y, Sehitoglu H. A model for rolling contact failure[J]. *Wear*, 1999, 224: 38-49.
- [22] Sehitoglu H, Jiang Y. Fatigue and stress analyses of rolling contact[A]. In: *Technical Report, Materials Engineering-Mechanical Behavior*[C]. University of Illinois at Urbana-Champaign, 1992: 161.
- [23] Fatemi A, Socie D F. A critical plane approach to multiaxial fatigue damage including out-of-phase loading[J]. *Fatigue & Fracture of Engineering Materials & Structures*, 1988, 11(3): 149-165.
- [24] Smith K N, atson P, Topper T H. A stress-strain function for the fatigue of metals[J]. *Journal of Materials*, 1970, 5(4): 767-778.
- [25] Arias O, Li Z, Lewis R, et al. Rolling-sliding laboratory tests of friction modifiers in dry and wet wheel-rail contacts[J]. *Wear*, 2010, 268(3): 543-551.
- [26] Zhang J Q. Fatigue Life Prediction Method for Continuous Tubing Based on Artificial Neural Networks [D]. Xi'an University of Petroleum, 2023.
- [27] Wang J B, Zeng L L, Yang K. Multi-objective optimization of printed circuit heat exchanger with airfoil fins based on the improved PSO-BP neural network and the NSGA-II algorithm[J]. *Nuclear Engineering and Technology*, 2023, 55(6): 2125-2138.